

Received October 31, 2019, accepted November 14, 2019, date of publication November 19, 2019, date of current version December 3, 2019.

Digital Object Identifier 10.1109/ACCESS.2019.2954081

A Novel Fast Retina Keypoint Extraction Algorithm for Multispectral Images Using Geometric Algebra

YANPING LI 

College of Information Engineering, Shanghai Maritime University, Shanghai 201306, China

e-mail: gmwlyp@126.com

This work was supported by the National Natural Science Foundation of China (NSFC) under Grant U1701265 and Grant 61771322.

ABSTRACT The feature extraction for multispectral images plays an important role in many computer vision applications. Recently, geometric algebra (GA) based scale invariant feature transform algorithm (GA-SIFT) and GA based speeded up robust Features algorithm (GA-SURF), have been proposed to extract feature of multispectral image in GA space. However those methods are difficult to be implemented in real-time applications. Now, the challenge is to design a new algorithm to extract the features of multispectral image more efficiently and quickly, so that it can be used in real-time applications. Although the proposed fast retina keypoint (FREAK) algorithm is faster to compute and more robust than SIFT and SURF, it can not be utilized to extract features directly for multispectral images. In this paper, we propose a novel fast retina keypoint extraction algorithm based on GA, named as GA-FREAK, for multispectral images. Firstly, the multispectral images are represented as multivectors in GA space, then the interest points are detected with the procedure of FREAK in GA space. Finally, our experiments demonstrate that the GA-FREAK is faster and more robust than some previous algorithms in multispectral images. It is expected that the proposed GA-FREAK will be a competitive alternative in real-time applications of multispectral images.


INDEX TERMS Fast retina keypoint (FREAK), geometric algebra (GA), feature extraction, multispectral image.

I. INTRODUCTION

Recently, multispectral images have been widely used in many fields, such as computer vision, biology, remote sensing, astronomy, medicine, and digital photography [1]–[7]. Multispectral images consist of various image data captured at specific wavelength ranges across the electromagnetic spectrum and have more than three bands to contain more information than grayscale images. Feature extraction analysis is becoming more and more popular in multispectral image applications [8], [9], and it is applied to many aspects, such as object recognition, image stitching, and pattern recognition [10], [11].

More and more research works focus on the design of effective feature extraction algorithms in embedded devices with restricted memory and computation. The scale invariant feature transform (SIFT) proposed by Lowe is one of the most popular feature extraction algorithm [12]. Many

SIFT based feature descriptors for color images are proposed, such as RGB-SIFT [13], HSV-SIFT [13], PCA-SIFT [14], and so on. However, SIFT based image feature extraction methods suffer from large computational burden. The speeded up robust feature (SURF) [15] proposed by Bay is a computationally-efficient replacement to SIFT, which outperforms SIFT in robustness and speed [16]. Since then, many algorithms based on SURF extensions are proposed, such as SURF-DAISY [17], Gauge-SURF [18], and SSURF [19]. Baig *et al.* [20] proposed a novel robust image representation for the content-based image retrieval (CBIR), which is based on complementary visual words intergration of SURF and cooccurrence histograms of oriented gradients (CoHOG). Mehmood *et al.* [21] proposed technique which carries visual words fusion of SURF and HOG features descriptors can give classification accuracy of 98.40%. Sharif *et al.* [22] proposed a novel approach, which relies on the fusion of visual words of SIFT and BRISK descriptors based on the visual-bag-of-words approach. Mehmood *et al.* [23] introduced two novel methods for effective image retrieval known as visual words

The associate editor coordinating the review of this manuscript and approving it for publication was Guitao Cao .

integration after clustering (VWlaC) and feature integration before clustering (FibC). Mehmood *et al.* [24] proposed a novel adapted triangular area-based technique, which computes local intensity order pattern (LIOP) features, weighted soft codebooks, and triangular histograms from the four triangular areas of each image. Sarwar *et al.* [25] proposed a novel method established on the bag-of-words (BoW) model, which perform visual words integration of the LIOP feature and local binary pattern variance (LBPV) feature to reduce the issue of the semantic gap and enhance the performance of the CBIR.

However, such algorithms can not be utilized to extract feature from multispectral image directly, which can lead to loss of spatial and spectral information in a multispectral image. To solve the problem that multispectral images features can not be extracted directly, Li *et al.* [26] proposed a new image feature extraction method in multispectral image, named GA-SIFT, which incorporates GA [27]–[37] theory into the traditional SIFT framework. Jabeen *et al.* [40] proposed a novel GA based speeded up robust feature method (GA-SURF).

GA-SIFT has a heavy computational costs while applied in feature extraction of multispectral images, which can not be implemented in real-time application. Although GA-SURF improves GA-SIFT in terms of computational efficiency and robustness, as is known, FREAK [39] is a new faster feature descriptor, which is faster and more robust than SIFT and SURF. Jabeen *et al.* [40] proposed a novel CBIR technique based on the visual words fusion of SURF and FREAK feature descriptors. However, the related FREAK algorithms are often applied for gray images, or color images, which can not be used in multispectral images processing directly. Therefore, in this paper, we propose a novel feature extraction algorithm for multispectral images which incorporate GA theory into the traditional FREAK algorithms, where the multispectral images are regarded as GA multivectors in GA space.

The major contributions lies in the following aspects. Firstly, we use GA multivector to represent multispectral images, and each blade of GA map to each spectral images channel of multispectral images, which can enhance correlation between channels in multispectral images. Secondly, We creatively combine GA with the FREAK algorithm inspired by the Human Visual System, and propose a fast, compact and robust keypoint descriptor for multispectral images.

The rests of this paper are organized as follows, section 2 introduces related work. Section 3 represents how to extract and describe the features by GA-FREAK algorithm. Section 4 provides the experiment analysis. Finally, section 5 concludes the paper.

II. RELATED WORK

A. THE FREAK ALGORITHMS

For the descriptor of the FREAK [39], similar to the retina sampling pattern, the algorithm draws on the structure

of human visual sub-region to obtain information. The distribution of the sample point of the descriptor is similar to that the retina receptor domain. The interest points are chosen as the center, and the position of the sampling points uniformly distributed over the center of the circle remaining, each sample point need to be smoothed to be less sensitive to noise. We use different kernels size for each sample point. For the FREAK algorithm, the interest points of image are detected using the FAST [41] algorithm. FIGURE 1 illustrates the topology of the receptive fields, where each circle describes the standard deviation of the Gaussian kernel of the corresponding sample points, and the descriptor is formed by cascading the intensity comparison results of the pair of sampling points.

The FREAK descriptor F is defined as

$$F = \sum_{0 \leq a \leq N} 2^a T(P_a) \tag{1}$$

$$T(P_a) = \begin{cases} 1 & \text{if } (I(P_a^{r_1}) - I(P_a^{r_2})) > 0 \\ 0 & \text{otherwise} \end{cases} \tag{2}$$

where P_a is a pair of receptive fields, $T(P_a)$ is equal to 0 or 1 according to $I(P_a^{r_1})$ and $I(P_a^{r_2})$, N denotes the size of the descriptor. $I(P_a^{r_1})$, $I(P_a^{r_2})$ is the smoothed intensity of the first and second receptive field of the P_a respectively.

If N is large enough, thousands of interest points result in a large descriptor, however many of the interest points are useless to represent an image, the descriptors need to be filtered by the retina-based algorithm [39] to learn the best interest points from trained data.

The sampling area around the FREAK descriptor generates a low-dimensional descriptor vector, and the sampling area of the FREAK descriptor center generates a high-dimensional descriptor vector, it can be proved that: the FREAK algorithm descriptor formation process is similar to the imaging mechanism of retina sampling pattern.

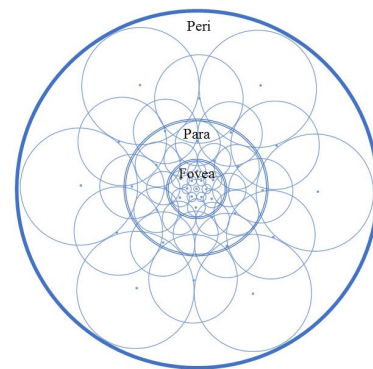


FIGURE 1. FREAK sampling pattern with its corresponding receptive fields [39].

B. THE BASICS OF GEOMETRIC ALGEBRA

Geometric algebra is a powerful and practical framework for the representation and solution of multi-dimensional

signal processing problems [30]–[37]. Let G_n denote the n -dimensions space of geometric algebra. The geometric product of a and b is described by the sum of a scalar and a bivector in GA space:

$$ab = a \cdot b + a \wedge b \quad (3)$$

where a and b denote vectors, $a \cdot b$ denotes the inner product of two vectors, and $a \wedge b$ denotes the outer product, and they are defined as

$$a \cdot b = \frac{1}{2}(ab + ba) \quad (4)$$

$$a \wedge b = \frac{1}{2}(ab - ba) \quad (5)$$

Besides, the n orthogonal basis vector is represented as e_1, e_2, \dots, e_n in GA space, the geometric product of basis vectors is described as

$$e_i \wedge e_j = -e_j \wedge e_i \quad i, j = 1, 2, \dots, n \quad (6)$$

$$e_i^2 = 1 \quad i, j = 1, 2, \dots, n \quad (7)$$

$$e_i \cdot e_j = \frac{1}{2}(e_i e_j + e_j e_i) \quad i, j = 1, 2, \dots, n \quad (8)$$

$$e_i e_j = e_i \cdot e_j + e_i \wedge e_j \quad (9)$$

In G_n , any an vector x can be denoted as $x = x_0 + \sum_{i=1}^n x_i e_i$.

A point object can be represented a multivector, which is composed of k -grade vector. A multivector can be represented as

$$M = \sum_A \partial_A e_A = \partial_0 + \sum_{i_1} \partial_{i_1} e_{i_1} + \sum_{i_1 \neq i_2} \partial_{i_1 i_2} e_{i_1 i_2} + \dots + \sum_{i_1 \neq i_2 \dots i_n} \partial_{i_1 i_2 \dots i_n} e_{i_1 i_2 \dots i_n} \quad (10)$$

where $A \in \{0, \oplus_{i_1} i_1, \oplus_{i_1 \neq i_2} i_1 i_2, \dots, \oplus_{i_1 \neq i_2 \dots i_n} i_1 i_2 \dots i_n\}$ and $\partial_A \in R$, G_n provides an efficient framework to conduct computations without using the coordinate information.

C. GA-SIFT ALGORITHM

GA-SIFT [26] enables image feature extraction to be applied in multispectral images. The multi-channel information is fully considered in multispectral images based on GA theory. The process is as follows.

Step 1: A multispectral image $f(x, y)$ is represented in GA space, each pixel represents a multivector.

$$f(x, y) = \sum_{i=1}^n f_i(x, y) e_i \quad (11)$$

where $f_i(x, y)$ is the i -th channel image of $f(x, y)$, and, n denotes the dimensions of the multispectral image.

Step 2: The scale of multispectral images L_C are obtained using the scale-varied Gaussian filter in GA space, then we can get GA-DoG images using L_C , which can be represented as:

$$L_C = \varphi(G_{n+2}(x, y, k \sum)) \otimes f(x, y) \otimes G_{n+2}(x, y, k \sum)$$

Step 3: The pixel value of the point in the GA-DoG images is compared to the surrounding pixel value, if it is the maximum or minimum, then the point is regarded as a interest point.

Step 4: The GA-SIFT descriptor for each interest point is generated with the magnitude and orientation.

D. GA-SURF ALGORITHM

Compared with GA-SIFT, GA-SURF algorithm [38] is faster and more robust, where the process of GA-SURF is defined as follows.

Step 1: The chromaticity image $\varphi(L(x, y))$ are extracted from an input multispectral image $f(x, y)$ in GA.

Step 2: The Hessian matrix is obtained in GA, the definition of the Hessian matrix is

$$H(x, y, \sigma) = \begin{bmatrix} \varphi(L_{xx}(x, y, \sigma)) & \varphi(L_{xy}(x, y, \sigma)) \\ \varphi(L_{xy}(x, y, \sigma)) & \varphi(L_{yy}(x, y, \sigma)) \end{bmatrix} \quad (13)$$

Then the determinant of the Hessian matrix is redefined as

$$\det(H) = \left| D(L_{xx}) \cdot D(L_{yy}) - \omega^2 D(L_{xy}) \cdot D(L_{xy}) \right| \quad (14)$$

where D_{xx} , D_{yy} and D_{xy} are the approximation of Gaussian second order derivatives using the box filter, ω is the weighted coefficient, which usually is set as 0.9.

Step 3: The image pyramid in GA space is mainly constructed to detect the interest point of the multispectral images by using scale-varied box filter, and the size of box filter is

$$Filter\ Size = 3 * (2^{octave} * interval + 1) \quad (15)$$

where the non-maximum suppression in a $3*3*3$ neighborhood is applied to localize the interest point in an image pyramids.

Step 4: The response value of the Haar wavelet in GA space is obtained using a slide orientation window, and the sum m_w and corresponding orientation of interest points is represented as

$$m_{w_x} = \sum_{i=1}^n \left(\sum_w dx \right) e_i \quad (16)$$

$$m_{w_y} = \sum_{i=1}^n \left(\sum_w dy \right) e_i \quad (17)$$

$$m_w = |m_{w_x} + m_{w_y}| \quad (18)$$

$$\theta_w = \arctan(|m_{w_x}| / |m_{w_y}|) \quad (19)$$

where dx and dy denote the response value of the Haar wavelet, w represents the slide orientation window, m_w is the maximum, and θ_w represents the dominant orientation of the interest point.

Step 5: The GA-SURF descriptor is described using Haar wavelet transform.

III. THE PROPOSED GA-FREAK ALGORITHM

A. THE MULTISPECTRAL IMAGES SCALE PYRAMID SPACE IN G_{n+2}

Refer to GA-SIFT [26] and GA-SURF [38], a multispectral image $f(x, y)$ in GA space is represented as Eq(11). The Gaussian filter G_{n+2} is introduced for multispectral images, the Gaussian filter is defined as:

$$G_{n+2}(x, y, \sum i) = \sum_i \left(\frac{1}{2\pi(\sum(i))^2} e^{-\frac{x^2+y^2}{2(\sum(i))^2}} \right) e_i \quad (20)$$

where $\sum(i)$ represents the standard deviation of the $n - th$ Gaussian filter, $n + 2$ represents the spectral information with n -dimensional coordinates in spectral space with the 2D coordinates in spatial space.

In practice, the Gaussian convolution kernel is often used in the convolution computation of the multi-channel images [26], [38], the Gaussian convolution kernel is defined as

$$G_{n+2} = \begin{pmatrix} g_{11} & g_{12} & \dots & g_{1N} \\ g_{21} & g_{22} & \dots & g_{2N} \\ \dots & \dots & \dots & \dots \\ g_{M1} & g_{M2} & \dots & g_{MN} \end{pmatrix} \quad (21)$$

where $g_{ij} = \sum_{k=1}^n g_{ijk} e_k$ and $g_{ijk} \in R$.

The scale space of a multispectral image can be generated by the convolution of the multispectral image and the Gaussian filter in G_{n+2} , then, the 2-side convolution of the multispectral image reflecting the relationship of spectral channels is provided as

$$\begin{aligned} L(x, y) &= G_{n+2}(x, y, \sigma_i) \otimes f(x, y) \otimes G_{n+2}(x, y, \sigma_i) \\ &= \left(\frac{1}{MN} \sum_{i=0}^{M-1} \sum_{j=0}^{N-1} (G_{n+2}(i, j, \sigma_i) f(x - i, y - j)) \right. \\ &\quad \left. \otimes G_{n+2}(x, y, \sigma_i) \right) \\ &= \frac{1}{M^2 N^2} \sum_{i=0}^{M-1} \sum_{j=0}^{N-1} \sum_{p=0}^{M-1} \sum_{q=0}^{N-1} (G_{n+2}(i, j, \sigma_i) \\ &\quad \times f(x - i - p, y - j - q) G_{n+2}(p, q, \sigma_i)) \quad (22) \end{aligned}$$

where M and N represents the size of the convolution window.

In order to simplify the forms of operation, we redefined $G_{n+2}(i, j, \sigma_i) = \sum_{i=1}^n g_i(i, j, \sigma_i) e_i$, $f(x - i - p, y - j - q) = \sum_{i=1}^n f_i(x - i - p, y - j - q) e_i$, and $G_{n+2}(p, q, \sigma_i) = \sum_{i=1}^n g'_i(p, q, \sigma_i) e_i$. Then we also replace $g_i(x, y, \sigma_i)$ with g_i , replace $f_i(x - i - p, y - j - q)$ with f_i , and replace $g'_i(p, q, \sigma_i)$ with g'_i . then the Eq.(22) can be transformed as

$$\begin{aligned} &G_{n+2}(x, y, \sigma_i) \otimes f(x, y) \otimes G_{n+2}(x, y, \sigma_i) \\ &= \frac{1}{M^2 N^2} \sum_{i=0}^{M-1} \sum_{j=0}^{N-1} \sum_{p=0}^{M-1} \sum_{q=0}^{N-1} \left(\left(\sum_{i=1}^n g_i e_i \right) \right. \\ &\quad \left. \times \left(\sum_{i=1}^n f_i e_i \right) \left(\sum_{i=1}^n g'_i e_i \right) \right) \end{aligned}$$

$$\begin{aligned} &= \frac{1}{M^2 N^2} \sum_{i=0}^{M-1} \sum_{j=0}^{N-1} \sum_{p=0}^{M-1} \sum_{q=0}^{N-1} \left(\sum_{k=0}^n \sum_{l=0}^n g_k g'_l f_k e_l \right) \\ &+ \frac{1}{M^2 N^2} \sum_{i=0}^{M-1} \sum_{j=0}^{N-1} \sum_{p=0}^{M-1} \sum_{q=0}^{N-1} \\ &\quad \times \left(\sum_{k=0}^n \sum_{l=0}^n \sum_{t=0}^n (g_k g'_l f_l (e_k \wedge e_l \wedge e_t)) \right) \quad (23) \end{aligned}$$

As is known, the second multivector cannot be applied directly to multispectral images, to simplify that, a function φ is introduced to get the first part of the Eq(23). We defined L_c to represent the scale space of the multispectral image as follows.

$$\begin{aligned} L_c &= \varphi(G_{n+2} \otimes f \otimes G_{n+2}) \\ &= \frac{1}{M^2 N^2} \sum_{i=0}^{M-1} \sum_{j=0}^{N-1} \sum_{p=0}^{M-1} \sum_{q=0}^{N-1} \left(\sum_{k=0}^n \sum_{l=0}^n g_k g'_l f_k e_l \right) \quad (24) \end{aligned}$$

B. GA-FREAK ALGORITHM FOR MULTISPECTRAL IMAGE

Consequently, The image Gaussian pyramid in GA space is constructed to detect the interest points in multispectral images. For the detection of interest points of multispectral images, the FAST algorithm [41] is introduced to detect interest points. In details, the FAST algorithm operates by considering a circle of sixteen pixels around the corner candidate p , if exists a set of n contiguous pixels in circle, which are larger than the pixel value of the candidate pixels I_p plus the threshold t , or smaller than the pixel value of the candidate pixels I_p minus the threshold t . Usually, we choose n equal to 12, because it can exclude a large number of non-corners: we first detect the four pixels at 1,5,9,13. If exists at least three points of pixels larger than $I_p + t$ or smaller than $I_p - t$ we determine p is a corner. If this is not the case, then p cannot be a corner. Next, we check the remaining pixels in the circle to determine if the points is really a candidate point. Then a corner response function V is introduced, and need to be computed for each candidate, and non-maximal suppression applied to remove the part of corner which have an adjacent corner with higher V . The definition of V is as follows:

$$\begin{aligned} V &= \max \left(\left| \sum_{i=1}^n \left(\sum_{x \in S_b} |I_{i(p \rightarrow x)} - I_{ip}| - t \right) e_i \right|, \right. \\ &\quad \left. \left| \sum_{i=1}^n \left(\sum_{x \in S_d} |I_i - I_{i(p \rightarrow x)}| - t \right) e_i \right| \right) \quad (25) \end{aligned}$$

where s_b, s_d respectively indicate the value of the points larger than $I_p + t$ or smaller than $I_p - t$ on the circle, I_i is the intensity of the i -th band image of multispectral images, e_i indicates an orthogonal basis in GA space. We compute the sum of the absolute difference between all points on the circle and the pixels in the center pixel.

After detection of the interest points, the retinal sampling pattern algorithm is utilized to describe the interest points.

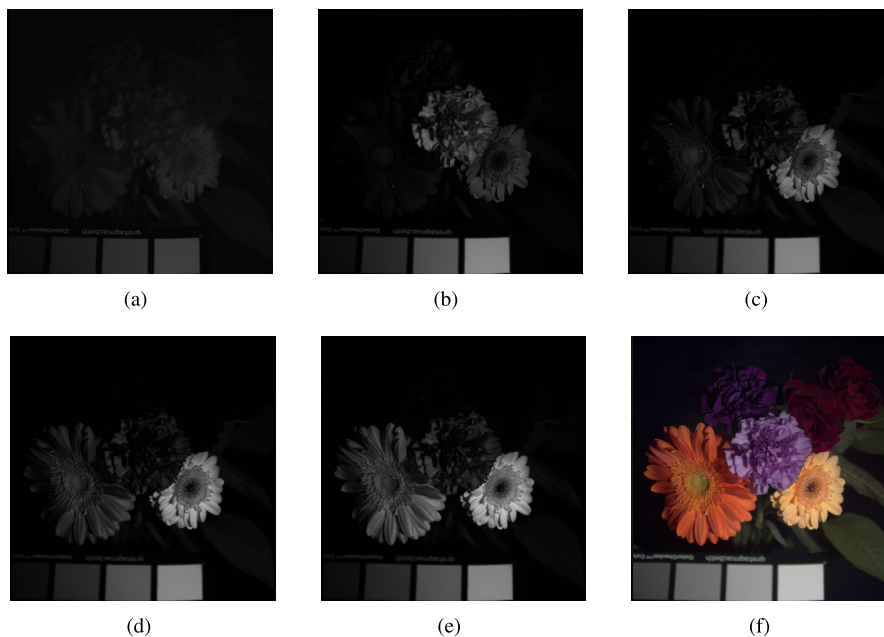


FIGURE 2. Testing on a multispectral image. (a) band-1 image. (b) band-2 image. (c) band-3 image. (d) band-4 image. (e) band-5 image. (f) color image.

A circular grid of retinal sampling with a difference in density points near the center is introduced. Then, each interest point must be smoothed to be less sensitive to noise, to match the Retina sampling pattern, where different kernel size of each interest point are used similar to BRISK [42]. FIGURE 1 shows the topology of the receptive field, each circle represents the standard deviations of the Gaussian kernels, the point at the center is the interest point extracted by the FAST algorithm, and the points around are extracted to generate descriptor.

After the above processing, the binary descriptor, a binary string is constructed as

$$F = \sum_{0 \leq a \leq N} 2^a T(P_a) \tag{26}$$

$$T(P_a) = \begin{cases} 1 & \text{if } \left(\left| \sum_{i=1}^n I_i(P_o^{r1}) e_i \right| - \left| \sum_{i=1}^n I_i(P_o^{r2}) e_i \right| \right) > 0 \\ 0 & \text{otherwise} \end{cases} \tag{27}$$

where P_a is a pair of receptive fields, and N denotes the size of the descriptor, $I(P_o^{r1})$ represents the smoothed intensity of the first receptive field of the pair P_a .

There are 43 points in FIGURE 1, which will generate 903 point pairs. Consequently, the retina-like algorithm to learn the best points pair is described as follows.

Step1. A matrix D of nearly fifty thousands of extracted keypoints is constructed, each row of the matrix corresponds to a keypoint descriptor.

Step2. The variance of each column is computed, the greater the variance, the more information the column carries, then the columns are sorted with respect to the highest variance.

Step3. Keep the best column (variance is the biggest) and iteratively add remaining columns which have low correlation with selected columns.

In order to make the generated descriptor with orientation invariance, we sum the estimated local gradients over selected point pairs, and select point pairs in symmetric receptive fields with respect to the center, the orientation formula is defined as follows.

$$O = \frac{1}{M} \sum_{p_o \in S} \left(\sum_{i=1}^n (I_i(P_o^{r1}) - I_i(P_o^{r2})) e_i \right) \frac{P_o^{r1} - P_o^{r2}}{\|P_o^{r1} - P_o^{r2}\|} \tag{28}$$

where S is the set of all point pairs, M is the number of the pairs in S , and P_o^{rj} is the 2D vector of spatial coordinates.

C. THE IMPLEMENTATION OF GA-FREAK

The proposed GA-FREAK algorithm is provided as follows.

Step1: The multispectral image $f(x, y)$ are represented in GA space, denoted as Eq(11).

Step2: The scale pyramid $L_c(x, y)$ is constructed in G_{n+2} space by Eq(24). Then we use FAST algorithm to detect the interest points.

Step3: Feature points are filtered by the retina-like algorithm.

Step4: features orientation are computed.

Step5: The descriptors of interest points are generated with orientation in GA space.

IV. EXPERIMENTS ANALYSIS

In this section, the experiments with on the color and multispectral images are implemented to verify the performance of the proposed GA-FREAK algorithm compared with FREAK, GA-SURF and GA-SIFT.

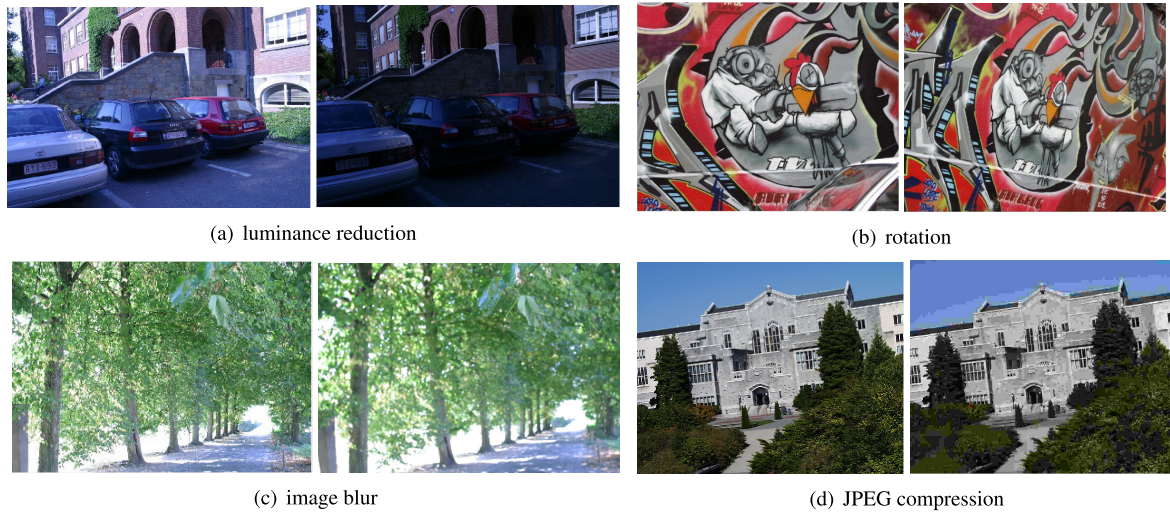


FIGURE 3. Testing on color images.

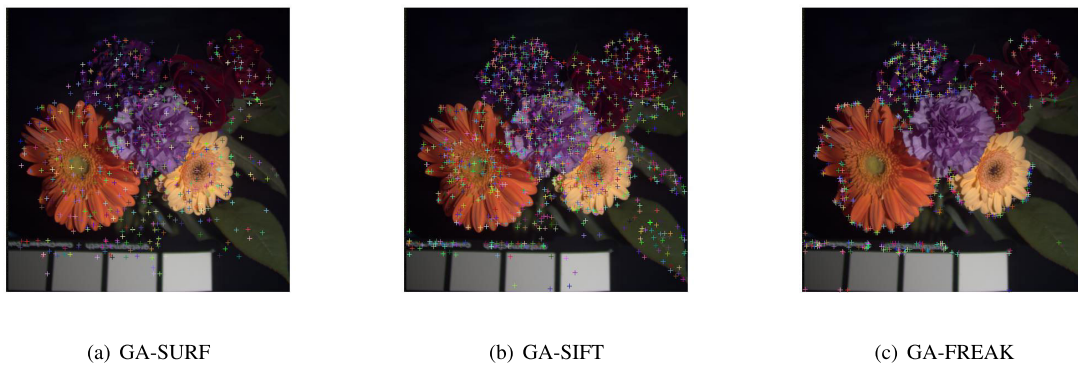


FIGURE 4. The interest points extracted from multispectral image using GA-SURF, GA-SIFT, GA-FREAK(n=31).

TABLE 1. The interest points analysis on multispectral images with different bands.

Number of bands(n)	GA-SURF		GA-SIFT		GA-FREAK	
	Interest points	Time(s)	Interest points	Time(s)	Interest points	Time(s)
n=4	331	4.03	472	9.49	512	0.92
n=5	348	4.06	565	10.86	643	1.08
n=6	364	4.17	618	11.90	695	1.15
n=31	489	4.79	1197	24.48	954	1.74

A. DATASETS

The two datasets, a color image dataset and a multispectral image dataset, are as follows.

We can get the multispectral image dataset in <http://www.cs.columbia.edu/CAVE/databases/multispectral/>. A multispectral image with 31 bands is chosen randomly to evaluate the performance of the GA-FREAK algorithm, and the color image and five simple band images are shown in FIGURE 2.

We can get the color image dataset in <http://www.robots.ox.ac.uk/vgg/data/data-aff.html>. We mainly choose four types of pictures, they are (1) luminance reduction, (2) image rotation, (3) image blur, (4) JPEG compression. We select two images for each types to test the performance, these

images are used in the experiment are shown in FIGURE 3. In the experiments, all algorithms are running on an Inter i5-65500 CPU@3.2G processor.

B. EXPERIMENTAL RESULTS

In this section, we evaluate the performance of GA-FREAK with FREAK, GA-SURF and GA-SIFT algorithm in feature extraction with different transformations using the two datasets. Refer to GA-SURF, GA-SIFT algorithms, the recall-precision is introduced as the metric to evaluate the performance of GA-FREAK, GA-SURF, GA-SIFT and FREAK algorithms. More information about the metrics of recall and 1-precision can be found in [26], [38].

TABLE 2. The interest points analysis on color images.

Algorithm	JPEG compression		Image blur		rotation		Luminance reduction	
	Interest points(correct-positive)	Time(s)(detect and match)	Interest points(correct-positive)	Time(s)(detect and match)	Interest points(correct-positive)	Time(s)(detect and match)	Interest points(correct-positive)	Time(s)(detect and match)
GA-SURF	920	12.93	931	20.47	375	12.49	795	13.59
GA-SIFT	935	68.09	881	224.79	609	70.47	554	44.87
FREAK	1465	0.78	1096	2.3	168	0.72	464	0.79
GA-FREAK	1294	0.76	874	1.11	366	0.76	341	0.72

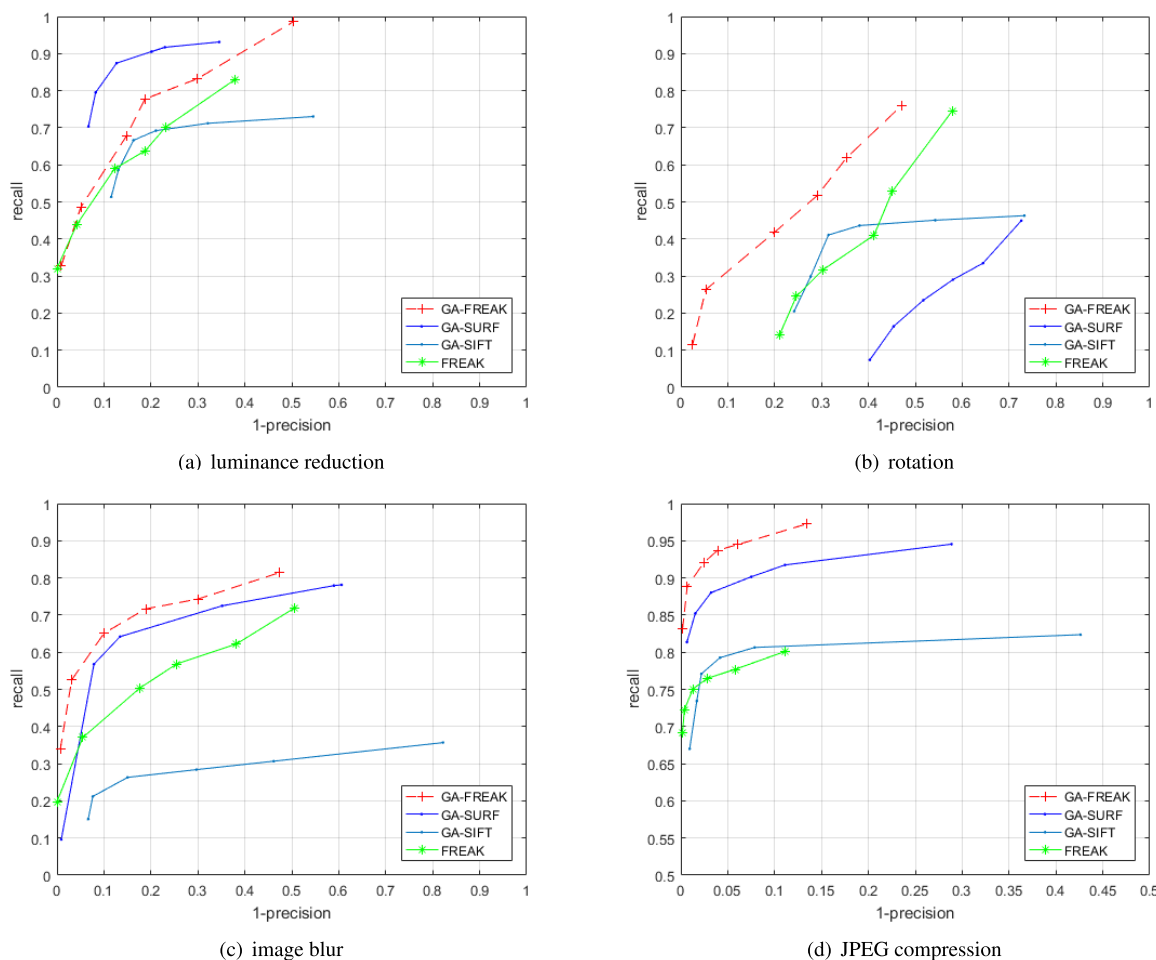


FIGURE 5. Comparisons of recall and 1-precision with different algorithms on color images.

1) PERFORMANCE ANALYSIS ON MULTISPECTRAL IMAGES
 In this section, we compare GA-FREAK with GA-SIFT, GA-SURF on multispectral images. For a multispectral image with 31 bands, FIGURE 4 shows the interest points extraction using GA-FREAK, GA-SURF, and GA-SIFT. The number of the interest points using GA-FREAK reaches 954, which is more than that of GA-SURF with 494. Table 1 shows the feature extraction from multispectral images with different bands by GA-FREAK, GA-SURF, and GA-SIFT. When the number of bands increases, the number of points extracted

is also increasing by the three algorithms. When the number of bands is equal to 4, the number of interest points using GA-FREAK reaches 512, more than 331 of GA-SURF and 472 of GA-SIFT. The detection time of the interest points by GA-FREAK is 0.92s, is faster than 4.03s of GA-SURF and 9.39s of GA-SIFT. When the number of band is 6, the number of interest points using GA-FREAK reaches 695, larger than 364 of GA-SURF and 618 of GA-SIFT, and the detection time of GA-FREAK is less than that of GA-SURF and GA-SIFT. For band-31 image, the number of interest

points using GA-FREAK reaches 954, large than 489 of GA-SURF, less than 1197 of GA-SURF, and the detection time of GA-FREAK is 1.74s, less than 4.98s of GA-SURF and 24.48s of GA-SIFT respectively. From the above analysis, we can find that GA-FREAK is faster than GA-SURF and GA-SIFT on multispectral images with considerable numbers of the interest points.

2) PERFORMANCE ANALYSIS ON COLORS IMAGES

In this section, we compare GA-FREAK with GA-SIFT, GA-SURF and FREAK on color images to evaluate the performance in feature extraction. The number of correct-positive interest points and the computational time are shown in table 2 from color images by different algorithms. From the result of experiments, GA-FREAK is the fastest among GA-SURF, GA-SIFT and FREAK on JPEG compression, Image blur and Luminance reduction. Besides, GA-FREAK can extract more correct features than GA-SURF and GA-SIFT on JPEG compression, which is 1294, 920 and 935 respectively. In Image blur, correct features by GA-FREAK is almost same as GA-SURF and GA-SIFT, while the time of GA-FREAK is the most lest. We can conclude that GA-FREAK is more effective than GA-SURF and GA-SIFT.

FIGURE 5 illustrates the comparisons of recall and 1-precision with different algorithms on color images with luminance reduction, rotation, image blur, and JPEG compression. On the luminance reduction, FIGURE 5(a) shows the performance of GA-FREAK is better than that of GA-SIFT and FREAK, when the images is distorted by reducing the luminance. FIGURE 5(b), FIGURE 5(c) and FIGURE 5(d) demonstrate that the performance of GA-FREAK is the best among GA-SURF, GA-SIFT and FREAK in the case of rotation, image blur and JPEG compression. Besides, FIGURE 5 shows that GA-FREAK outperforms FREAK in all color images, the reason is that GA-FREAK can retain inherent spectral structures completely, and enhance the correlation between the three channels of the color images.

V. CONCLUSIONS

In this paper, we have proposed a novel geometric algebra based fast retina keypoint descriptor for multispectral images, denoted as GA-FREAK, where the GA theory is introduced to detect and describe the local interest points of multispectral images. Thanks to GA theory, the scale of the multispectral images can be obtained by calculating the 2-side convolution. Then the interest points are detected by FAST algorithm in GA space, the score function is used to remove the part of corner which have an adjacent corner with higher score, the feature descriptors are generated finally in GA space. Experimental results have shown that GA-FREAK is faster to compute and more robust than GA-SIFT, GA-SURF and FREAK in most cases. At next steps, we will pay more attention to various applications using GA-FREAK algorithm.

REFERENCES

- [1] X. Shen, L. Xu, Q. Zhang, and J. Jia, "Multi-modal and multi-spectral registration for natural images," in *Proc. Eur. Conf. Comput. Vis.* Cham, Switzerland: Springer, 2014, pp. 309–324.
- [2] Q. Xie, Q. Zhao, D. Meng, Z. Xu, S. Gu, W. Zuo, and L. Zhang, "Multispectral images denoising by intrinsic tensor sparsity regularization," in *Proc. IEEE Conf. Comput. Vis. Pattern Recognit. (CVPR)*, Jun. 2016, pp. 1692–1700.
- [3] S. Bernab, P. R. Marpu, A. Plaza, M. D. Mura, and J. A. Benediktsson, "Spectral-spatial classification of multispectral images using kernel feature space representation," *IEEE Geosci. Remote Sens. Lett.*, vol. 11, no. 1, pp. 288–292, Jan. 2014.
- [4] G. Vivone, R. Restaino, M. Dalla Mura, G. Licciardi, and J. Chanussot, "Contrast and error-based fusion schemes for multispectral image pansharpening," *IEEE Geosci. Remote Sens. Lett.*, vol. 11, no. 5, pp. 930–934, May 2014.
- [5] Y. Hao, Z. Sun, T. Tan, and C. Ren, "Multispectral palm image fusion for accurate contact-free palmprint recognition," in *Proc. IEEE Int. Conf. Image Process.*, Oct. 2008, pp. 281–284.
- [6] S. M. Hamylton, J. D. Hedley, and R. J. Beaman, "Derivation of high-resolution bathymetry from multispectral satellite imagery: A comparison of empirical and optimisation methods through geographical error analysis," *Remote Sens.*, vol. 7, no. 12, pp. 16257–16273, 2015.
- [7] C. Du and S. Gao, "Remote sensing image fusion based on nonlinear IHS and fast nonsubsampling contourlet transform," *J. Indian Soc. Remote Sens.*, vol. 46, no. 12, pp. 2023–2032, 2018.
- [8] R. Chen, X. Lin, and T. Ding, "Liveness detection for iris recognition using multispectral images," *Pattern Recognit. Lett.*, vol. 33, no. 121, pp. 1513–1519, Sep. 2012.
- [9] Q. Zhang, Z. Cao, Z. Hu, Y. Jia, and X. Wu, "Joint image registration and fusion for panchromatic and multispectral images," *IEEE Geosci. Remote Sens. Lett.*, vol. 12, no. 3, pp. 467–471, Mar. 2015.
- [10] W. Cao, J. Yuan, Z. He, Z. Zhang, and Z. He, "Fast deep neural networks with knowledge guided training and predicted regions of interests for real-time video object detection," *IEEE Access*, vol. 6, pp. 8990–8999, 2018.
- [11] W. Cao, Q. Lin, Z. He, and Z. He, "Hybrid representation learning for cross-modal retrieval," *Neurocomputing*, vol. 345, pp. 45–57, Jun. 2019.
- [12] D. G. Lowe, "Object recognition from local scale-invariant features," in *Proc. 7th IEEE Int. Conf. Comput. Vis.*, Sep. 1999, pp. 1–8.
- [13] K. E. A. van de Sande, T. Gevers, and C. G. M. Snoek, "Evaluating color descriptors for object and scene recognition," *IEEE Trans. Pattern Anal. Mach. Intell.*, vol. 32, no. 9, pp. 1582–1596, Sep. 2010.
- [14] Y. Ke and R. Sukthankar, "PCA-SIFT: A more distinctive representation for local image descriptors," in *Proc. IEEE Conf. Comput. Vis. Pattern Recognit.*, Jun/Jul. 2004, pp. 1–8.
- [15] H. Bay, A. Ess, T. Tuytelaars, and L. V. Gool, "SURF: Speeded up robust features," in *Proc. Eur. Conf. Comput. Vis.* Berlin, Germany: Springer, 2006, pp. 404–417.
- [16] R. Kalia, K.-D. Lee, B. V. R. Samir, S. K. Je, and W.-G. Oh, "An analysis of the effect of different image preprocessing techniques on the performance of SURF: Speeded up robust features," in *Proc. 17th Korea-Japan Joint Workshop Frontiers Comput. Vis. (FCV)*, Feb. 2011, pp. 1–6.
- [17] L. Li and J. Zic, "Image matching algorithm based on feature-point and DAISY descriptor," *J. Multimedia*, vol. 9, no. 6, pp. 829–835, 2014.
- [18] P. F. Alcantarilla, L. M. Bergasa, and A. J. Davison, "Gauge-SURF descriptors," *Image Vis. Comput.*, vol. 31, no. 1, pp. 103–116, 2013.
- [19] M. Du, J. Wang, J. Li, H. Cao, G. Cui, J. Fang, J. Lv, and X. Chen, "Robot robust object recognition based on fast SURF feature matching," in *Proc. Chin. Automat. Congr.*, Nov. 2013, pp. 581–586.
- [20] F. Baig, Z. Mehmood, and M. Rashid, "Boosting the performance of the BoVW model using SURF-CoHOG-based sparse features with relevance feedback for CBIR," in *Proc. Iranian J. Sci. Technol., Trans. Elect. Eng.*, Jul. 2019, pp. 1–20.
- [21] Z. Mehmood, F. Abbas, T. Mahmood, M. A. Javid, A. Rehman, and T. Nawaz, "Content-based image retrieval based on visual words fusion versus features fusion of local and global features," *Arabian J. Sci. Eng.*, vol. 43, pp. 7265–7284, Dec. 2018.
- [22] U. Sharif, Z. Mehmood, T. Mahmood, M. A. Javid, A. Rehman, and T. Saba, "Scene analysis and search using local features and support vector machine for effective content-based image retrieval," *Artif. Intell. Rev.*, vol. 52, no. 2, pp. 901–925, Aug. 2019.

- [23] Z. Mehmood, M. Rashid, A. Rehman, T. Saba, H. Dawood, and H. Dawood, "Effect of complementary visual words versus complementary features on clustering for effective content-based image search," *J. Intell. Fuzzy Syst. Preprint*, vol. 35, no. 5, pp. 5421–5434, Nov. 2018.
- [24] Z. Mehmood, N. Gul, M. Altaf, T. Mahmood, T. Saba, A. Rehman, and M. T. Mahmood, "Scene search based on the adapted triangular regions and soft clustering to improve the effectiveness of the visual-bag-of-words model," *EURASIP J. Image Video Process.*, vol. 2018, Jun. 2018, Art. no. 48, doi: [10.1186/s13640-018-0285-7](https://doi.org/10.1186/s13640-018-0285-7).
- [25] A. Sarwar, Z. Mehmood, and T. Saba, "A novel method for content-based image retrieval to improve the effectiveness of the bag-of-words model using a support vector machine," *J. Inf. Sci.*, vol. 45, pp. 117–135, Feb. 2019, doi: [10.1177/0165551518782825](https://doi.org/10.1177/0165551518782825).
- [26] Y. Li, W. Liu, X. Li, Q. Huang, and X. Li, "GA-SIFT: A new scale invariant feature transform for multispectral image using geometric algebra," *Inf. Sci.*, vol. 281, pp. 559–572, Oct. 2014.
- [27] W. Rui, S. Miaomiao, W. Xiangyang, and C. WenMing, "RGA-CNNs: Convolutional neural networks based on reduced geometric algebra," *Sci. China Inf. Sci.*, to be published, doi: [10.1007/s11432-018-1513-5](https://doi.org/10.1007/s11432-018-1513-5).
- [28] A. Chapman and U. Vishne, "Clifford algebras of binary homogeneous forms," *J. Algebra*, vol. 366, no. 15, pp. 94–111, Sep. 2012.
- [29] V. Labunets, "Clifford algebras as unified language for image processing and pattern recognition," in *Computational Noncommutative Algebra and Applications*, vol. 136. Amsterdam, The Netherlands: Springer, 2004, pp. 197–225.
- [30] T. Batard, C. Saint-Jean, and M. Berthier, "A metric approach to nD images edge detection with clifford algebras," *J. Math. Imag.*, vol. 33, no. 3, pp. 296–312, 2009.
- [31] Y. S. Li, "A digital image watermarking algorithm based on clifford algebra," *Acta Electronica Sin.*, vol. 36, no. 5, pp. 852–855, 2008.
- [32] S. Buchholz and G. Sommer, "On clifford neurons and clifford multi-layer perceptrons," *Neural Netw.*, vol. 21, no. 7, pp. 925–935, Sep. 2008.
- [33] R. Wang, Y. He, C. Huang, X. Wang, and W. Cao, "A novel least-mean kurtosis adaptive filtering algorithm based on geometric algebra," *IEEE Access*, vol. 7, pp. 78298–78310, 2019.
- [34] R. Wang, M. Shen, T. Wang, and W. Cao, "L1-Norm Minimization for Multi-dimensional Signals Based on Geometric Algebra," *Adv. Appl. Clifford Algebras*, vol. 29, p. 33, Apr. 2019.
- [35] R. Wang, M. Shen, and W. Cao, "Multivector sparse representation for multispectral images using geometric algebra," *IEEE Access*, vol. 7, pp. 12755–12767, 2019.
- [36] W. Cao, F. Lyu, Z. He, G. Cao, and Z. He, "Multimodal medical image registration based on feature spheres in geometric algebra," *IEEE Access*, vol. 6, pp. 21164–21172, 2018.
- [37] M. Shen, R. Wang, and W. Cao, "Joint sparse representation model for multi-channel image based on reduced geometric algebra," *IEEE Access*, vol. 6, pp. 24213–24223, 2018.
- [38] R. Wang, Y. Shi, and W. Cao, "GA-SURF: A new speeded-up robust feature extraction algorithm for multispectral images based on geometric algebra," *Pattern Recognit. Lett.*, vol. 15, pp. 11–17, Nov. 2019, doi: [10.1016/j.patrec.2018.11.001](https://doi.org/10.1016/j.patrec.2018.11.001).
- [39] A. Alahi, R. Ortiz, and P. Vanderghenst, "FREAK: Fast retina keypoint," in *Proc. IEEE Conf. Comput. Vis. Pattern Recognit.*, Jun. 2012, pp. 510–517.
- [40] S. Jabeen, Z. Mehmood, and T. Saba, "An effective content-based image retrieval technique for image visuals representation based on the bag-of-visual-words model," *PLoS ONE*, vol. 13, Apr. 2018, Art. no. e0194526, doi: [10.1371/journal.pone.0194526](https://doi.org/10.1371/journal.pone.0194526).
- [41] E. Rosten and T. Drummond, "Machine learning for high-speed corner detection," in *Proc. Eur. Conf. Comput. Vis. (Lecture Notes in Computer Science)*, vol. 3951. Berlin, Germany: Springer, 2006, pp. 430–443.
- [42] S. Leutenegger, M. Chli, and R. Y. Siegwart, "Brisk: Binary robust invariant scalable keypoints," in *Proc. IEEE Int. Conf. Comput. Vis. (ICCV)*, Barcelona, Spain, Nov. 2011, pp. 2548–2555.

• • •